

7. Conclusion

7.1 Variable Stars

Fitting a model to any variable stars in the dataset, so that this model could be subtracted from the data to leave a constant baseline, has only been partially successful. In total, the program detected 322 variable stars – a much lower number than was expected. As can be seen from Figure 4, some variable stars in the dataset have been successfully modelled, and when the model is subtracted from the data a reasonably constant baseline is left. On the other hand, some variable stars have not been modelled accurately, as shown by Figure 26.

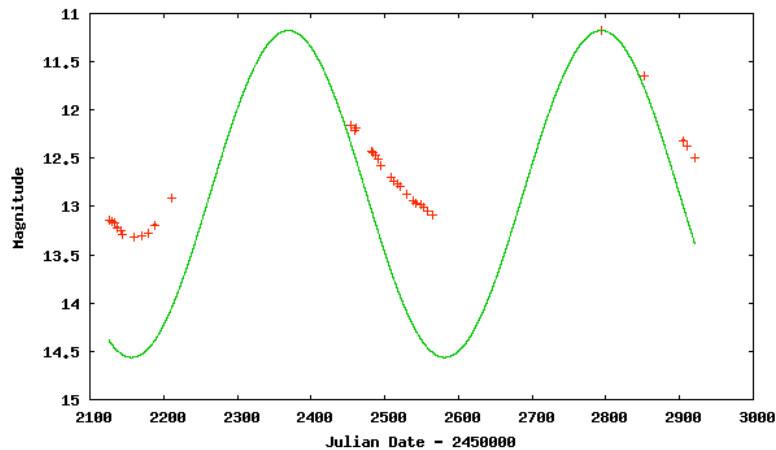


Figure 26: Star #82869: an example of a bad fit of the model to a variable star

This could be due to several factors, the most important of which being the period of the star. The star in Figure 4 has a relatively short period of around 50 days, so it has been observed through more periods than the star in Figure 26, which has a larger period of around 430 days. This means that the fitting program has more ‘oscillations’, which results in a more accurate model. Also, longer period stars are less likely than short period stars to have data points covering an entire period, due to the gaps in the dataset between viewing seasons. This can be clearly seen in Figure 26. The solution to this is to use a larger data set, taken over an expanded period of time – ideally much longer than the period of the stars, as any microlensing event occurring in a variable star will cause problems with accurately fitting the model. If an event were present, it would be advisable to fit the model to dataset in two halves, ensuring that the candidate event is contained in only one of the halves, and use the one with the lowest χ^2 .

An alternative reason could be due to the nature of short period variable stars (5 to 90 days), which are generally more sinusoidal than those with longer periods (>150 days). As our model has only three sine and three cosine terms, it is much better at fitting the simpler, short period models. A solution to this would be to use a more complicated complete model. This would increase processing time, but could be vital in detecting microlensing events in variable stars. Ideally, multiple models could be fitted to the variable light curve, with the best fit with the lowest number of terms being used to normalize the light curve.

Overall, while normalizing has not been entirely successful in this project, it could be expanded to be a useful tool for future searches.

7.2 Microlensing Search Routines

The microlensing search routines used in this report have generally worked well, and returned good results. There is, however, scope for a number of refinements to the processes that would improve their ability to detect microlensing events, and reduce the number of false-positives they return.

The OGLE routine has the advantage that it quickly identifies the bulk of the microlensing events. The main problem with this technique is that it ideally requires a data set covering a larger amount of time than that used here, due to the window of 50% of the data set that is used to identify if a star is constant before and/or after a microlensing event. With a reduced window size, the method detects more events, but at the cost of flagging an increased number of false positives. The other methods used would also see reliability increases on a larger data set.

While the Least Squares Fitting searching technique returns the best ratio of microlensing events to false-positives, it is rather slow, taking approximately 6-10 times the processing time of the OGLE technique.¹ If sufficient processing power is available, however, this is probably the best of the techniques used here. This technique has the capacity to be optimized, both in terms of speed and accuracy, through improvements to the mathematics and code used, and refinements to the required limits on the variables. It could also be expanded to fit binary, and more exotic, microlensing events, with relative ease.

The number of points either side of the peak method has a number of flaws; it currently does not take into account errors on the magnitude measurements, and it cannot detect more exotic events like binary lenses. This method does not distinguish between types of events, so ideally a Least Squares fit should be applied to candidate light curves to verify that the flagged event is a microlensing event.

Overall, the best method would be the OGLE modified technique, or equivalently the OGLE routine when unmodified if it were run on a longer data set. The method with the most potential for use in the future, however, is the Least Squares Fitting method.

An additional technique to test would be MACHO’s search methods, described in Alcock et al. (2000). These have not been used in this report due to problems with translating the MACHO cuts from fluxes (in units of ADUs) to magnitudes.

7.3 Optical Depth

Method	Optical Depth
OGLE	$(5.7 \pm 1.5) \times 10^{-6}$
OGLE modified	$(4.3 \pm 1.0) \times 10^{-6}$
Least Squares Fit	$(6.9 \pm 1.4) \times 10^{-6}$
Number of Points	$(7.2 \pm 1.3) \times 10^{-6}$

Table 4: Summary of the optical depths for the various methods

The optical depths found in this data set, summarized in Table 4, are higher than expected; Alcock et al. (2000) gives their value of the optical depth to be $\tau_2^{300} = 2.43_{-0.29}^{+0.31} \times 10^{-6}$. There are a few potential reasons for this difference; in this report, worse sampled microlensing events have been taken into account than would normally be, and a smaller data set has been used, resulting in a smaller sampling of microlensing events.

Acknowledgements

Our thanks go to our supervisor, Dr. Mao, for his guidance, and to the OGLE-III collaboration for kindly providing the data used in this project.

¹ When running the OGLE technique, the bottleneck appeared to be the hard drive access speeds rather than the processing power, while the Least Squares Fitting uses a lot more processing power. It is likely that the ratio of the performances of these techniques will be larger if this bottleneck were removed.

References

- Alcock, C., et al., 2000, 'The MACHO Project: Microlensing Optical Depth towards the Galactic Bulge from difference image analysis', *The Astrophysical Journal*, **541**, pp. 734-766
- Galassi, M., et al., 2005; 'GNU Scientific Library Reference Manual', Edition 1.7 for GSL Version 1.7
- Glynn, E., Mushegian, A., 2004, 'Searching for Periodic Gene Expression Patterns using Lomb-Scargle Periodograms'
(Website: <http://research.stowers-institute.org/efg/2004/CAMDA/>)
- Jaroszyński, M., Paczyński, B., 1996, 'Global Energy Conservation in Gravitational Lensing', *Acta Astronomica*, **46**, pp. 361-376
- Mao, S., 1999, 'Gravitational Microlensing: Past, Present and Future', Boston Lensing Conference
(arXiv PrePrint: astro-ph/9909302)
- Paczynski, B., 1996, *Annual Reviews of Astronomy and Astrophysics*, **34**, 419
(arXiv PrePrint: astro-ph/9604011)
- Press, W. H., Teukolsky, S. A., Vetterling, W. T. and Flannery, B. P., 1992, 'Numerical Recipes in C', Second Edition, ISBN 0-521-43108-5.
- Udalski, A., 2003, 'The Optical Gravitational Lensing Experiment. Real Time Data Analysis in the OGLE-III Survey', *Acta Astronomica*, **53** 291
(arXiv PrePrint: astro-ph/0401123)
OGLE EWS online at <http://www.astrouw.edu.pl/~ogle/ogle3/ews/ews.html>
- Wambsgans, J., 2005, 'Gravitational Microlensing', Proceedings of the 33rd Saas-Fee Advanced Course
(Downloaded from <http://www.astro.uni-bonn.de/~peter/SaaSfee.html>)
- Woźniak, P. R., 2000, 'Difference Image Analysis of the OGLE-II Bulge Data. I, The Method', *Acta Astronomica*, **50**, 421
(arXiv PrePrint: astro-ph/0012143)
- Woźniak, P. R. et al., 2001, 'Difference Image Analysis of the OGLE-II Bulge Data. II. Microlensing Events', *Acta Astronomica*, **51**, pp175-219

Software

The program written for this project requires several additional libraries to be available, namely;

- GNU Scientific Library (GSL); <http://www.gnu.org/software/gsl/>
- GNUPlot; <http://www.gnuplot.info/>; installed with dependencies:
 - o LibGD, with dependencies:
 - Freetype2
 - LibJPEG
 - LibPNG
 - zlib
- GNUPlot C Interface, N. Devillard, <http://ndevilla.free.fr/gnuplot/>

It is also likely to be incompatible with Microsoft Windows as it requires dirent.h for directory listings, and the GNUPlot C Interface requires UNIX pipes.

Appendix A – Differentials for Least Squares Fitting

A.1 Differentials of Microlensing Model

The differentials used in the Least Squares fitting routine for the microlensing model are:

$$\frac{dm}{dt_{\text{peak}}} = \frac{dm}{d\mu_B} \frac{d\mu_B}{d\mu} \frac{d\mu}{dr} \left(-\frac{1}{r} \frac{t - t_{\text{peak}}}{t_E^2} \right)$$

$$\frac{dm}{dt_E} = \frac{dm}{d\mu_B} \frac{d\mu_B}{d\mu} \frac{d\mu}{dr} \left(-\frac{1}{r} \frac{(t - t_{\text{peak}})^2}{t_E} \right)$$

$$\frac{dm}{du_{\text{min}}} = \frac{dm}{d\mu_B} \frac{d\mu_B}{d\mu} \frac{d\mu}{dr} \frac{u_{\text{min}}}{r}$$

$$\frac{dm}{dm_b} = 1; \quad \frac{dm}{df_1} = \frac{dm}{d\mu_B} (\mu - 1)$$

with the ‘standard’ differentials:

$$\frac{dm}{d\mu} = -\frac{2.5}{\mu_B} \log_{10} e; \quad \frac{d\mu_B}{d\mu} = f_1$$

$$\frac{d\mu}{dr} = \frac{2r}{r\sqrt{r^2 + 4r}} - \frac{\left(\frac{r^2}{2} + 1\right)(4r^3 + 8r)}{\sqrt[3]{r^4 + 4r^2}}$$

A.2 Differentials of Period Model

As with fitting the microlensing model, equation (4.1) has to be differentiated with respect to the seven variable parameters M , A_i , B_i , P and t_0 . These differentials are;

$$\frac{dM}{dm_b} = 1$$

$$\frac{dM}{dA_i} = \sin(ix); \quad \frac{dM}{dB_i} = \cos(ix)$$

$$\frac{dM}{dP} = \frac{x}{P} \left(\sum_{i=1}^3 -iA_i \cos(ix) + iB_i \sin(ix) \right)$$

$$\frac{dM}{dt_0} = \frac{2\pi}{P} \left(\sum_{i=1}^3 -iA_i \cos(ix) + iB_i \sin(ix) \right)$$

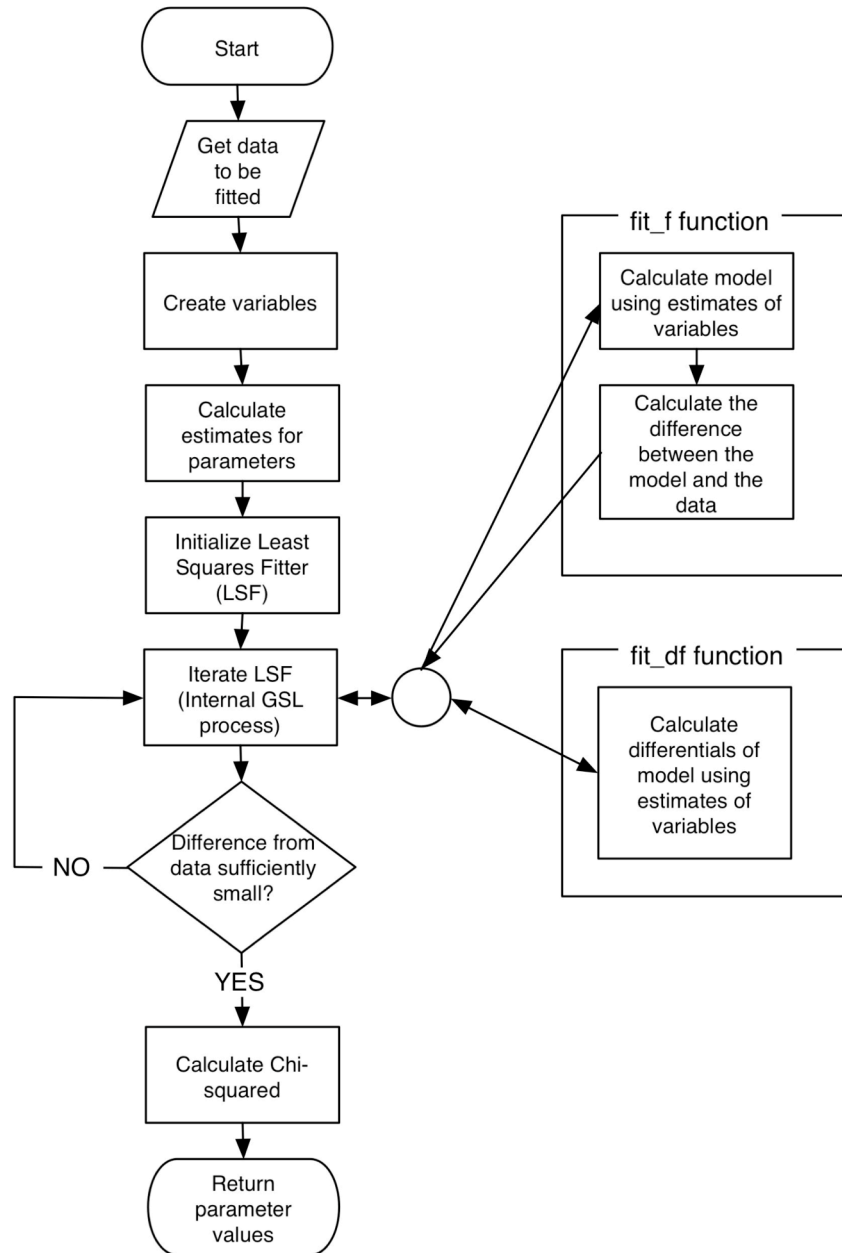
where $x = 2\pi(t - t_0) / P$.

Appendix B – Program Structure

The program code is available in the ‘Program’ directory of the enclosed DVD. The flowcharts below can be found in the ‘flowcharts’ directory.

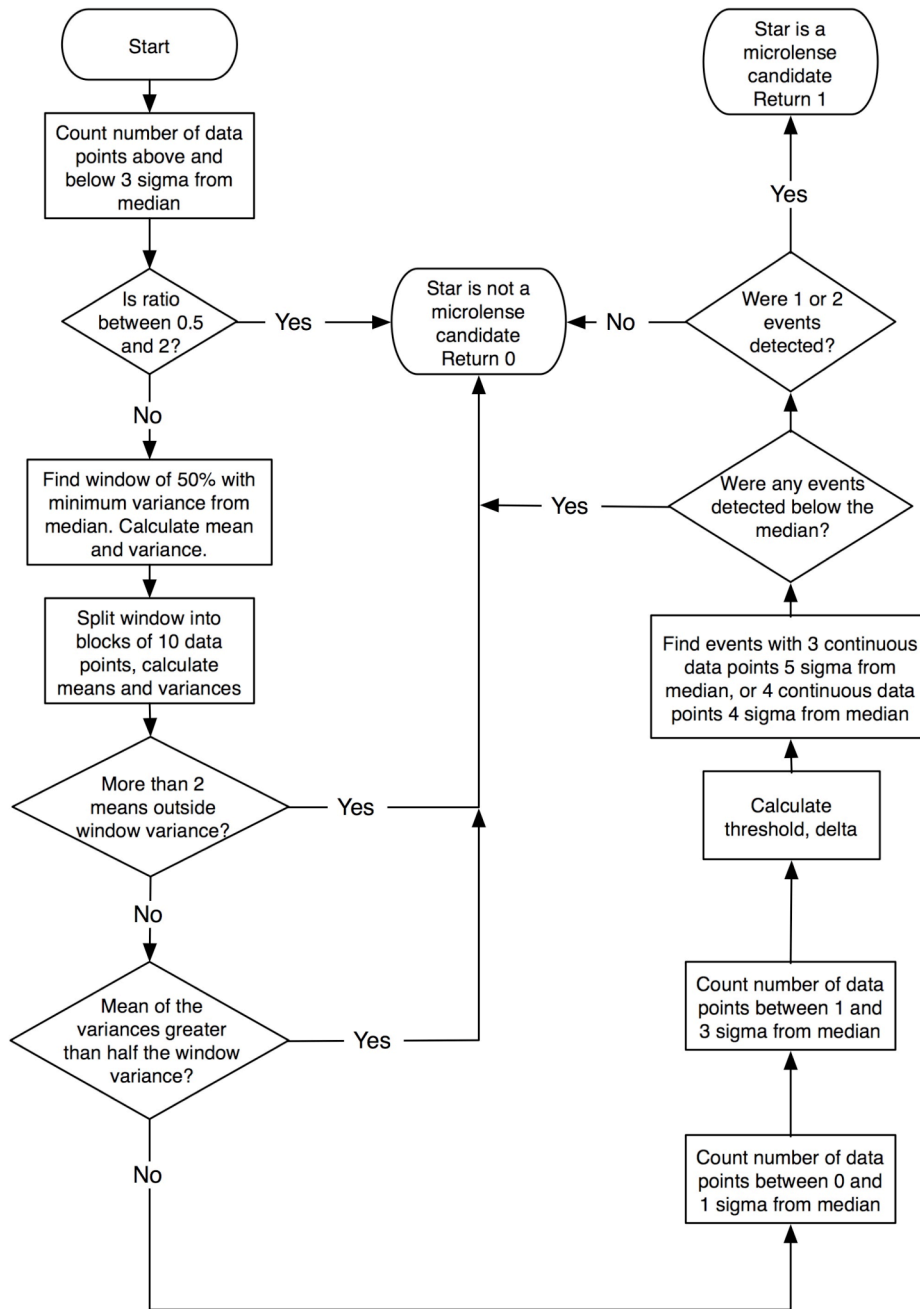
B.1 Least Squares Fitting Routine

Used in the fit_model and fit_period functions (fit.c and fit_period.c respectively)



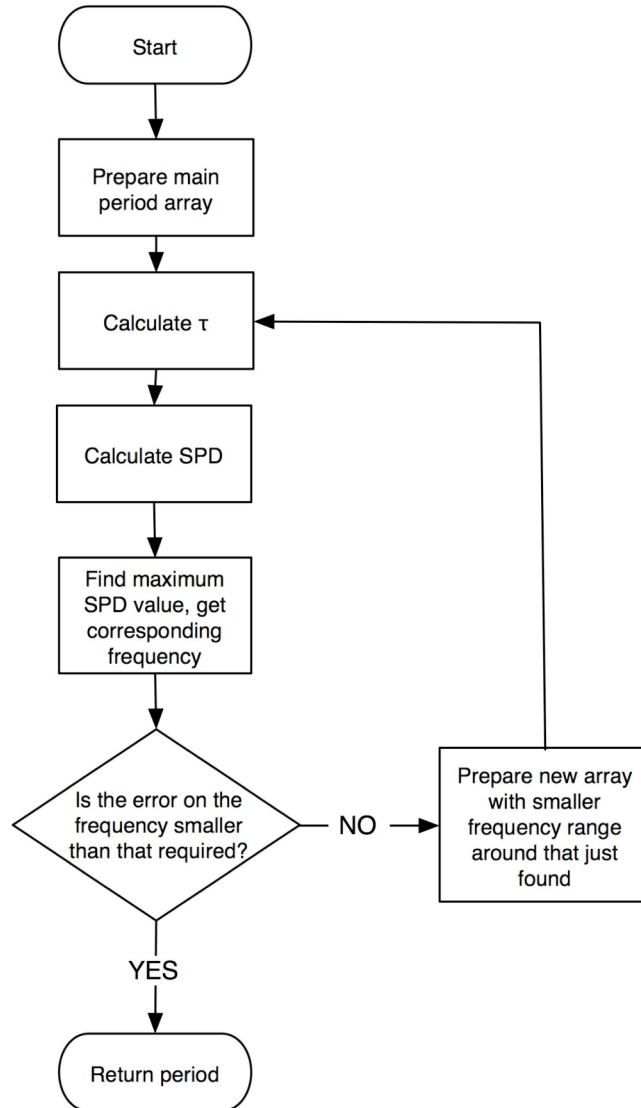
B.2 OGLE Search Criteria

Used in the identify_candidate function (candidates.c).



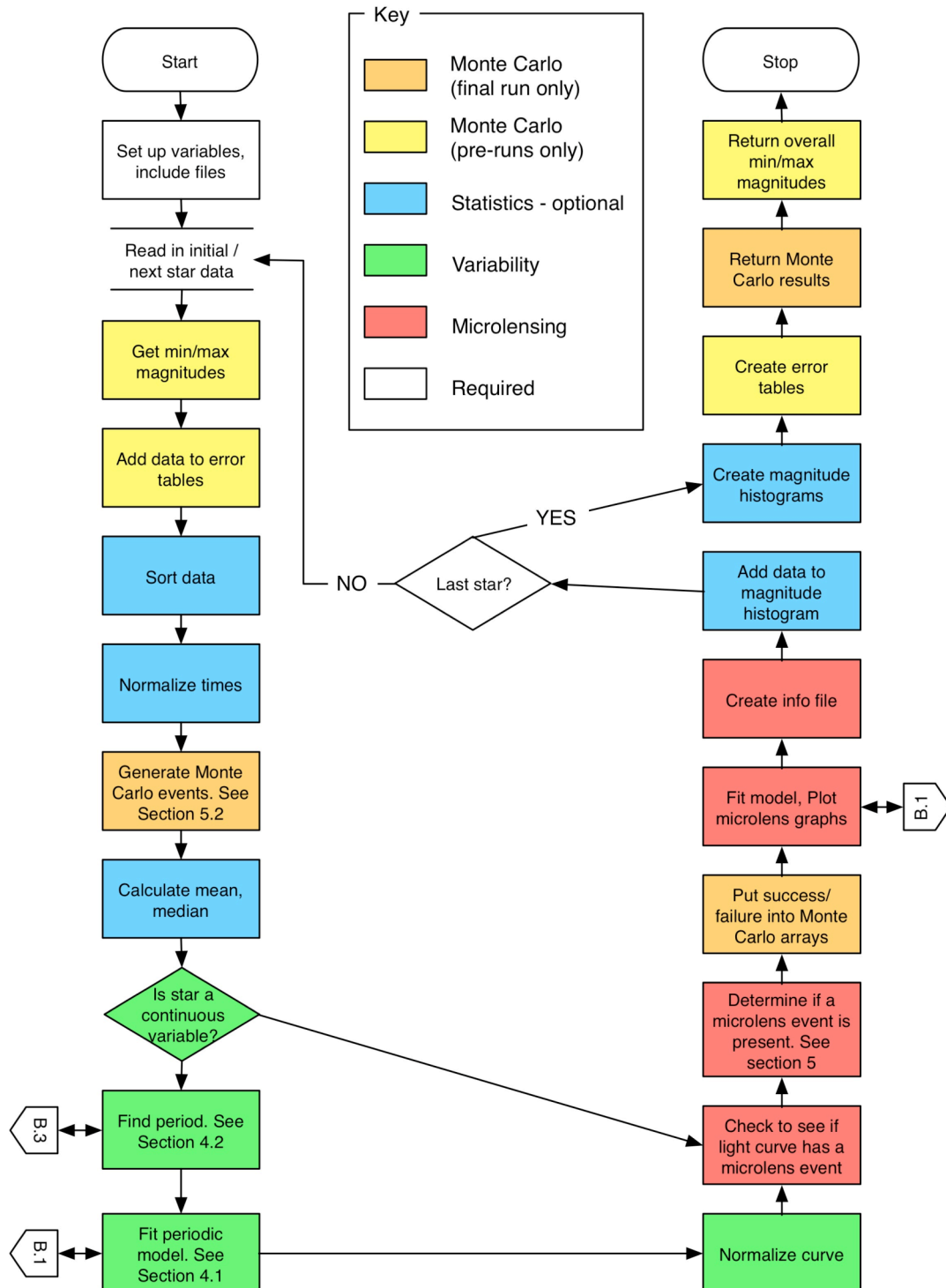
B.3 Lomb-Scargle Routine

Used in the find_period function in period.c



B.4 Main Program

Outline of main program, in main.c.



Appendix C – Systematic Errors

A potential source of systematic errors in this report is the effects of ‘seeing’ in the original data set. The result of these effects can be identified by looking at the distribution of magnitudes at different observation times. If a large number of stars are used to calculate this, then the effects of variable stars, microlensing events etc. are negligible. Figures C1 and C2 show the results of this analysis, performed on the full data set of 170,000 stars. The white areas are where no stars with that magnitude were found.

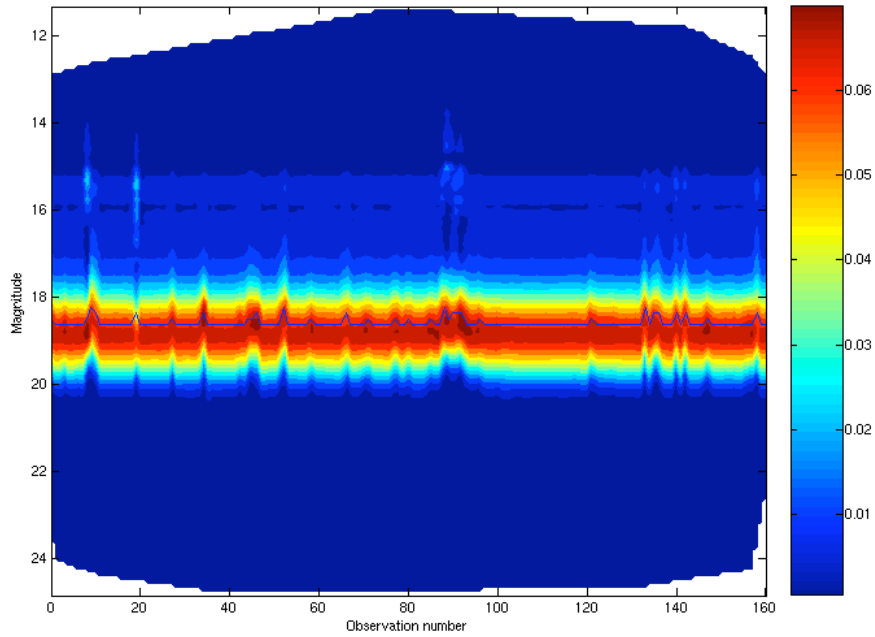


Figure C1: A 3D histogram of magnitudes vs. observation number for the light curves in our sample. The z axis is split into 160 bins, and normalized to 1, for each observation time. The blue line in the middle represents the median value.

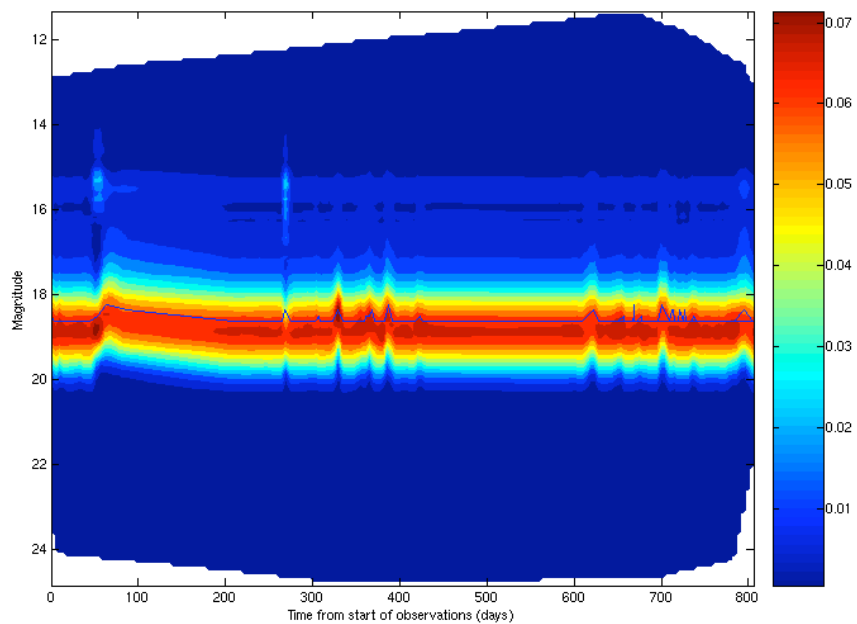


Figure C2: as Figure C1, but with the number of days from the start of the observations on the x-axis. No observations were taken between days 86 and 208, and 439 and 583.

One way of counteracting the errors that result from seeing is to increase the error bars on the measurements. Figures C3 and C4 show how the errors on different magnitudes vary with time. It can be seen from these that the shifts in magnitudes showed in figures C1 and C2 have not been fully counteracted by alterations in the errors on the magnitudes.

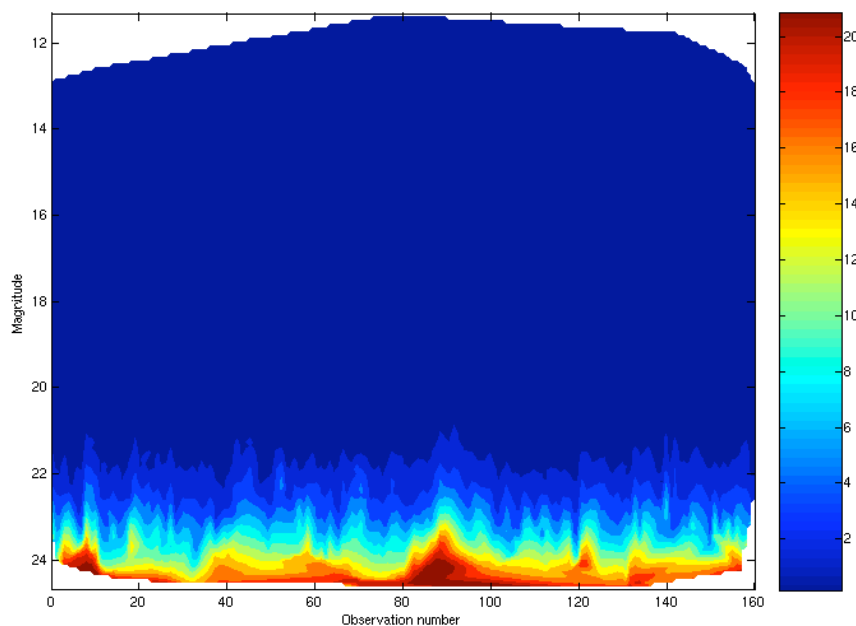


Figure C3: A 3D plot of magnitudes vs. observation number for the errors on the light curves in our sample. Blue indicates a small average error; red indicates a large average error.

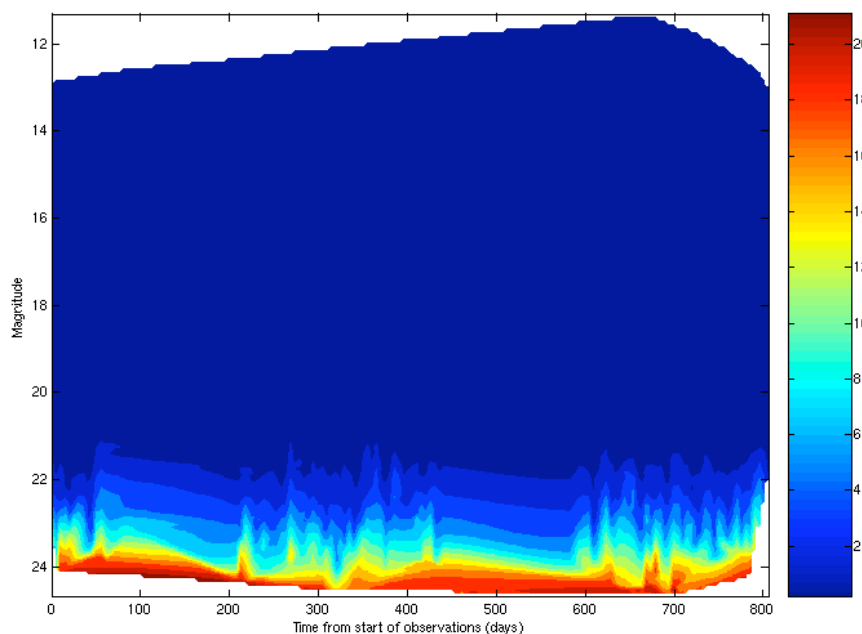


Figure C4: as Figure C3, but with time on the x-axis. No observations were taken between days 86 and 208, and 439 and 583.

From these diagrams, it can be seen that there are changes in the magnitudes of the stars in bulk over short periods, however over the long terms the magnitudes remain roughly constant. It is interesting that ‘magnitude islands’ appear in the data, where a large number of stars have clumped into similar magnitudes. It is possible that this has resulted from parts of the sky being surveyed becoming brighter, resulting in large numbers of stars from the range 18-20 magnitudes being given increased magnitudes.

It is also of interest that the boundaries of the magnitudes changes with time; at the start of the observations, magnitudes range between 13 and 24; this range increases to a maximum of 11.5 to 24.5, before decreasing to 13 to 22 at the end of the observations. It is unknown why this has occurred.